PHYSICAL REVIEW B **72**, 195336 (2005)

Cherenkov radiation of terahertz surface plasmon polaritons from a superluminal optical spot

M. I. Bakunov,[1,2] A. V. Maslov,[3] and S. B. Bodrov[1,2]
[1]*Department of Radiophysics, University of Nizhny Novgorod, Nizhny Novgorod 603950, Russia*
[2]*Institute of Applied Physics, Russian Academy of Sciences, Nizhny Novgorod, 603950, Russia*
[3]*Center for Nanotechnology, NASA Ames Research Center, MS 229-1, Moffett Field, California 94035, USA*
(Received 13 July 2005; revised manuscript received 4 October 2005; published 23 November 2005)

We propose to use a cylindrically focused ultrashort laser pulse obliquely incident on a semiconductor surface to launch surface plasmon polaritons with frequencies in the terahertz range. The laser pulse creates a spot of nonlinear polarization moving along the semiconductor surface with superluminal velocity. We show theoretically that the spot will emit the surface and free-space waves via Cherenkov mechanism. We develop a theory and calculate the radiated fields and frequency distribution of the radiated energy. The efficiency of the optical-to-terahertz conversion is estimated for the case of nonlinear optical rectification in GaAs. We show that one can control the radiation pattern and spectrum of the surface waves by varying the incident angle of the optical beam and crystalline orientation of the semiconductor. This technique opens new ways to build terahertz sources and perform surface spectroscopy.

DOI: 10.1103/PhysRevB.72.195336 PACS number(s): 42.65.Ky, 73.20.Mf, 78.47.+p

I. INTRODUCTION

The ultrafast current creation[1–3] and optical rectification[4,5] are proven techniques for generating terahertz (THz) radiation from semiconductor surfaces using short optical pulses. In both cases the resultant THz pulse propagates from the optical spot as free-space radiation with a broad spectrum. We propose and analyze a technique that can generate THz radiation that propagates along the semiconductor surface. As we show in this paper, this technique can produce THz fields with large amplitudes and offers THz tuning.

The general idea behind the optical-to-THz conversion is to create polarization (or current) that varies on the time scale of a few hundred femtoseconds. This polarization acts as a source of THz radiation. Let us assume that the surface at which THz generation occurs can guide surface waves, for example, surface plasmon polaritons (SPPs). If an incident optical pulse creates nonlinear polarization near the surface, the polarization can, in principle, generate not only free-space radiation, but also SPPs. However, a normally incident and weakly focused pulse, needed to maximize the excitation area, cannot excite surface waves. This is simply because the contributions from different regions of the optical spot interfere destructively for a spot size greater than the THz wavelength. A strongly focused pulse, on the other hand, can create a pointlike source capable of emitting into surface waves. Apparently, the conversion efficiency should be small because of the small area of the excitation spot.

Alternatively, one can use obliquely incident optical pulses. If a weakly focused optical pulse impinges obliquely upon a plane surface, the optical spot moves along the surface with superluminal velocity. Since the surface waves are slow (their phase velocity is less than the speed of light), the superluminal source should be pointlike to excite the Cherenkov cone (wedge) of surface waves. Therefore, the pulse should be strongly focused in the transverse (relative to the plane of incidence) direction, e.g., by a cylindrical lens. This situation is a two-dimensional analog of the generation of free-space THz waves by a moving pulse of nonlinear polarization in a homogeneous electro-optic medium.[6–9] A common problem limiting the power of the generated THz radiation in homogeneous materials is the large absorption coefficients ($\gtrsim 20\ \mathrm{cm}^{-1}$) at the THz frequencies.[10,11] The use of surfaces, rather than bulk materials, allows one to reduce the large absorption losses for THz waves when they are localized mostly outside of the semiconductor.

In this study, we focus explicitly on one type of surface waves—SPPs—that can be guided by the surface of a sufficiently doped semiconductor due to plasma contribution to the dielectric constant from the free carriers. The SPP propagation constant h is determined by the formula[12] $h=(\omega/c)[\varepsilon/(\varepsilon+1)]^{1/2}$, where ω is the SPP frequency, c is the speed of light, and $\varepsilon=\varepsilon_0[1-\omega_p^2\omega^{-1}(\omega-i\nu)^{-1}]$ is the dielectric function of the semiconductor with ε_0 the low-frequency dielectric constant, ω_p the plasma frequency, and ν the dephasing rate for electrons. Despite a rather high ratio $\nu/\omega \sim 0.1$ for typical semiconductors, SPPs of the THz frequency range can propagate long distances along the surface. This occurs if the plasma frequency ω_p significantly exceeds the wave frequency ω so that the skin depth in the semiconductor is sufficiently small and the SPP fields are localized predominantly in vacuum, rather than in the semiconductor. As a result, Ohmic losses are strongly reduced and the propagation length of SPPs $L_{\mathrm{SPP}}=(2\ \mathrm{Im}\, h)^{-1}$ can reach the centimeter range. For example, for GaAs with $\omega_p/2\pi=8$ THz, $\nu=2\ \mathrm{ps}^{-1}$, and $\varepsilon_0=12.9$, the propagation length of SPP can be estimated as $L_{\mathrm{SPP}}\approx 1$ cm for $\omega/2\pi=3$ THz and even $L_{\mathrm{SPP}}\approx 2.7$ cm for $\omega/2\pi=2$ THz.

Due to the strong localization of SPPs near the guiding surface, they are extremely sensitive to surface properties, a circumstance that makes SPPs a useful tool for surface studies. Infrared and visible SPPs guided by metal (Ag, Au) surfaces are widely used for biosensoring,[13] detecting surface contamination,[14] and other applications. Similarly, one can envision a different type of spectroscopy at semiconductor surfaces using the THz excitation technique we present here. In particular, one can scan a semiconductor surface using an

1098-0121/2005/72(19)/195336(9)/$23.00

©2005 The American Physical Society

optical laser beam and use the THz surface waves excited by the beam to measure the response from the surface in the THz frequency range. Two-dimensional THz micro-optics on semiconductor surfaces, analogous to SPPs optics on metal surfaces in the visible range,[15] can also be developed.

In this paper, we describe the main features of the THz surface wave generation using optical spots. In particular, we describe frequencies of the generated radiation, emission diagrams, and expected power yield. To be specific, we will assume that the optical spot creates a moving pulse of nonlinear polarization through optical rectification in the semiconductor. Other mechanisms, such as current surges, will also give rise to the creation of moving sources of radiation and, subsequently, to the generation of THz waves. The use of different mechanisms to create a moving source will affect mostly the conversion efficiency but not the main properties of the generated THz waves. Some preliminary results were reported in Ref. 16.

The paper is organized as follows. In Sec. II, we formulate the problem and lay out the basic equations. The solution of the equations using a Fourier-transform technique is given in Sec. III. In Sec. IV, we study the radiation pattern for the excited surface waves and estimate the power and energy conversion efficiencies. Free-space Cherenkov radiation is considered in Sec. V. Section VI contains concluding remarks.

II. EXCITATION SCHEME AND THEORETICAL MODEL

Our aim is the excitation of SPPs at the surface of a doped semiconductor with free-carrier concentration N. SPPs exist in the frequency range $0<\omega<\bar{\omega}_p$; $\bar{\omega}_p=\omega_p(1+\varepsilon_0^{-1})^{-1/2}$ is the maximal frequency, $\omega_p=\sqrt{4\pi e^2 N/(m\epsilon_0)}$ is the plasma frequency, ε_0 is the background dielectric constant of the semiconductor, and e and m are the electron charge and effective mass, respectively. High-frequency SPPs have very small phase velocities, while low-frequency SPPs have their phase velocities close to the speed of light in vacuum. To excite SPPs via the Cherenkov effect we need to create a source of polarization that moves faster than their phase velocities. To achieve that we propose to illuminate the surface with an obliquely incident optical pulse that produces a moving spot on the surface. We can further rely on optical rectification to create a polarization distribution that essentially reproduces the shape of the spot. Such a moving pulse of nonlinear polarization should generate SPPs. To ensure a sufficiently long distance scanned by the optical spot on the surface, the optical beam is weakly focused in the plane of incidence. At the same time it is strongly focused by a cylindrical lens in the direction transverse to this plane to satisfy the Cherenkov condition (Fig. 1). Due to weak focusing of the beam in one direction, we may approximate it as infinite in this direction. Thus, the optical spot created by the pulse on the semiconductor surface moves uniformly in the $+z$ direction with velocity $V=\beta c$, where $\beta=1/\sin\alpha$ and α is the angle of incidence (Fig. 1). We further note that since $V>c$ in this scheme, SPPs at all possible frequencies between 0 and $\bar{\omega}_p$ will be excited. For spots with $V<c$, only the SPPs with smaller phase velocities (and at high frequencies) would be excited. In such a regime, one can actually achieve phase matching between the spot and a copropagating SPP. The spot in this case no longer needs to be small in the transverse direction.[17]

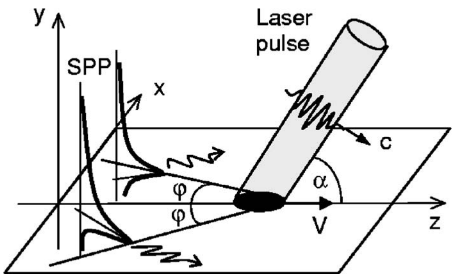

FIG. 1. Excitation scheme for surface plasmon polaritons (SPP): an obliquely incident laser pulse produces an optical spot that moves with velocity $V=c/\sin\alpha$ along the semiconductor surface and excites the Cherenkov cone of SPPs. The thick solid lines show schematically the exponential profiles of the SPPs.

If the optical pulse is at frequency higher than the bandgap, the optical energy (and nonlinear polarization) will be localized near the surface within the depth much smaller than the wavelength of the THz radiation that we want to excite. Thus, the created nonlinear polarization can be written as

$$\mathbf{P}_{\mathrm{NL}}=\mathbf{p}F(\xi)G(x)\delta(y), \tag{1}$$

with $\delta(y)$ the usual delta function. The function $G(x)=\exp(-x^2/\ell_\perp^2)$ describes the transverse size of the optical beam; the function $F(\xi)$ is the time-dependent envelope of the intensity of the optical pulse, and $\xi=t-z/V$. The new variable ξ reflects the uniform motion of the spot along z. For all estimates we assume the Gaussian envelope:

$$F(\xi)=\exp(-\xi^2/\tau^2), \tag{2}$$

where τ is the pulse duration (the standard FWHM pulse duration is $\tau_{\mathrm{FWHM}}=2\sqrt{\ln 2}\,\tau$). The orientation of the amplitude vector $\mathbf{p}$ is determined by the polarization of the optical beam and orientation of the crystallographic axes of the sample. We will consider the general case with all three components p_x, p_y, and p_z included.

The nonlinear polarization $\mathbf{P}_{\mathrm{NL}}$ acts as a superluminal dipole that excites free-space and surface waves. The surface waves propagate from the optical spot along the semiconductor surface $y=0$ and form the usual Cherenkov cone (wedge) in this plane. The pattern of the excited surface waves can be represented as a superposition of plane surface waves propagating under different angles φ (see Fig. 1). Each partial wave has an in-plane wave vector h and angular frequency ω that are determined by matching the phase velocity of the wave along the z axis $v_z^{\mathrm{ph}}=\omega/(h\sin\varphi)$ and the velocity of the optical spot V (see Figs. 2(a) and 2(b)). This matching condition gives the cone angle $\varphi<\alpha$ in which surface waves exist.

The radiation generated by the moving nonlinear polarization $\mathbf{P}_{\mathrm{NL}}$ can be found from Maxwell's equations, which have the following form for the fields in the semiconductor $(y<0)$:

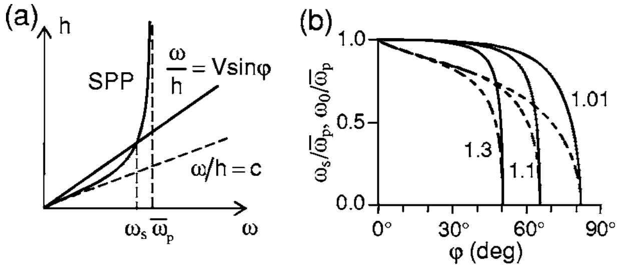

FIG. 2. (a) Kinematic diagram (in-plane wave number h versus frequency ω) which illustrates phase-matching between the moving nonlinear source and the generated SPP. The intersection of the dispersion curve for SPP and the line $\omega/h = V\sin\varphi$ gives the frequency ω_s of the partial SPP propagating at the angle φ. The maximal frequency for SPPs is $\bar{\omega}_p = \omega_p(1+\varepsilon_0^{-1})^{-1/2}$. (b) Normalized frequency $\omega_s/\bar{\omega}_p$ (solid lines) of the partial surface wave and stationary frequency $\omega_0/\bar{\omega}_p$ (dashed lines) as functions of φ for $\varepsilon_0 = 12.9$ (GaAs) and $\beta = 1.01$, 1.1, and 1.3 (values shown near corresponding curves).

$$\boldsymbol{\nabla}_\xi \times \mathbf{E} = -\frac{1}{c}\frac{\partial \mathbf{B}}{\partial \xi}, \tag{3a}$$

$$\nabla_\xi \times \mathbf{B} = \frac{\varepsilon_0}{c}\frac{\partial \mathbf{E}}{\partial \xi} - \frac{4\pi}{c} eN\mathbf{v} + \frac{4\pi}{c}\mathbf{j}_{\mathrm{NL}}, \tag{3b}$$

where the nabla operator $\boldsymbol{\nabla}_\xi$ has components ($\partial/\partial x$, $\partial/\partial y$, $-V^{-1}\partial/\partial\xi$) and $\mathbf{j}_{\mathrm{NL}} = \partial \mathbf{P}_{\mathrm{NL}}/\partial\xi$ is the nonlinear current. The equation for electron motion is

$$m\frac{\partial \mathbf{v}}{\partial \xi} = -e\mathbf{E}. \tag{4}$$

In Eq. (4), we neglected collisions that do not affect our results significantly if the excited SPPs have small damping. We also neglected the contributions to the currents from the optically created carriers for two reasons. First, the carriers are created only in a narrow and thin (compared to the SPP's wavelength) strip behind the optical spot. Second, their density is assumed to be small compared to the background density N. In vacuum ($y>0$), we use Eqs. (3a) and (3b) with $N=0$ and $\varepsilon_0 = 1$.

III. SOLUTION IN FOURIER DOMAIN

To solve Eqs. (3a), (3b), and (4), we apply Fourier transforms with respect to ξ and x to these equations. We arrive at the following equations for the field Fourier transforms (ω and g are the Fourier variables that correspond to ξ and x, respectively):

$$\frac{\partial \tilde{E}_x}{\partial y} + ig\tilde{E}_y = \frac{i\omega}{c}\tilde{B}_z, \quad \frac{\partial \tilde{E}_z}{\partial y} + \frac{i\omega}{V}\tilde{E}_y = -\frac{i\omega}{c}\tilde{B}_x,$$

$$\frac{i\omega}{V}\tilde{E}_x - ig\tilde{E}_z = \frac{i\omega}{c}\tilde{B}_y,$$

$$\frac{\partial \tilde{B}_z}{\partial y} + \frac{i\omega}{V}\tilde{B}_y = \frac{i\omega\varepsilon}{c}\tilde{E}_x + \frac{4\pi i\omega}{c}\tilde{G}\tilde{F}\delta(y)p_x, \tag{5}$$

$$ig\tilde{B}_z - \frac{i\omega}{V}\tilde{B}_x = \frac{i\omega\varepsilon}{c}\tilde{E}_y + \frac{4\pi i\omega}{c}\tilde{G}\tilde{F}\delta(y)p_y,$$

$$-\frac{\partial \tilde{B}_x}{\partial y} - ig\tilde{B}_y = \frac{i\omega\varepsilon}{c}\tilde{E}_z + \frac{4\pi i\omega}{c}\tilde{G}\tilde{F}\delta(y)p_z,$$

where the dielectric function $\varepsilon(y,\omega)$ is $\varepsilon_p = \varepsilon_0(1-\omega_p^2/\omega^2)$ in the semiconductor ($y<0$) and unity in vacuum ($y>0$), $\tilde{G}(g) = (\ell_\perp/2\sqrt{\pi})\exp(-g^2\ell_\perp^2/4)$ is the Fourier transform of $G(x)$, and $\tilde{F}(\omega)$ is the Fourier transform of $F(\xi)$. For example, for the Gaussian pulse (2) we have

$$\tilde{F}(\omega) = \frac{\tau}{2\sqrt{\pi}}\exp\left(-\frac{\omega^2\tau^2}{4}\right). \tag{6}$$

We proceed by solving Eqs. (5) in the homogeneous regions ($y<0$ and $y>0$). The solutions are a superposition of p-polarized waves with

$$\tilde{B}_y = 0, \quad \tilde{E}_y = \begin{cases} C_v \exp(-\kappa_v y), & y>0, \\ C_p \exp(\kappa_p y), & y<0, \end{cases} \tag{7}$$

and s-polarized waves with

$$\tilde{E}_y = 0, \quad \tilde{B}_y = \begin{cases} D_v \exp(-\kappa_v y), & y>0, \\ D_p \exp(\kappa_p y), & y<0, \end{cases} \tag{8}$$

where $\kappa_v = [g^2 - \omega^2 c^{-2}(1-\beta^{-2})]^{1/2}$ and $\kappa_p = [g^2 - \omega^2 c^{-2}(\varepsilon_p - \beta^{-2})]^{1/2}$. Other field components in the waves can be found by using Eqs. (5). We match the solutions (7) and (8) by the boundary conditions

$$[\tilde{B}_z] = \frac{4\pi i\omega}{c}\tilde{G}\tilde{F}p_x, \quad [\tilde{B}_x] = -\frac{4\pi i\omega}{c}\tilde{G}\tilde{F}p_z, \quad [\tilde{B}_y] = 0,$$

$$[\tilde{E}_x] = \frac{4\pi i g}{\varepsilon_p}\tilde{G}\tilde{F}p_y, \quad [\tilde{E}_z] = \frac{4\pi i\omega}{V\varepsilon_p}\tilde{G}\tilde{F}p_y, \tag{9}$$

that arise after integrating the equations across the boundary at $y=0$; the square brackets denote the change of the enclosed quantity at the interface $y=0$, for example, $[\tilde{B}_x] = \tilde{B}_x|_{y=0^+} - \tilde{B}_x|_{y=0^-}$. We note that the component $\tilde{E}_y$ behaves like $\sim\delta(y)$ due to the presence of p_y.

As a result, we arrive at the following expressions for the mode amplitudes:

$$C_v = \frac{4\pi\tilde{G}\tilde{F}}{\Delta}\left[\left(g^2 + \frac{\omega^2}{V^2}\right)p_y + i\kappa_p\left(gp_x + \frac{\omega}{V}p_z\right)\right], \tag{10a}$$

$$C_p = \frac{4\pi\tilde{G}\tilde{F}}{\Delta}\left[\left(g^2 + \frac{\omega^2}{V^2}\right)\frac{p_y}{\varepsilon_p} - i\kappa_v\left(gp_x + \frac{\omega}{V}p_z\right)\right], \tag{10b}$$

$$D_v = D_p = \frac{4\pi\omega\tilde{G}\tilde{F}}{c(\kappa_v + \kappa_p)}\left(\frac{\omega}{V}p_x - gp_z\right), \tag{10c}$$

where $\Delta(\omega) = \varepsilon_p\kappa_v + \kappa_p$.

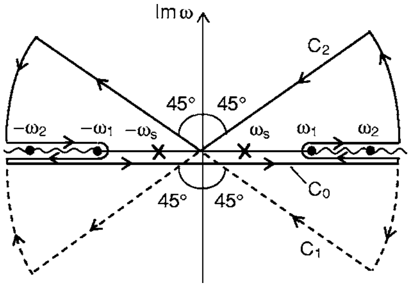

FIG. 3. Singularities and paths of integration in the complex ω plane for the inverse Fourier transform. The branch points $\omega = \pm\omega_{1,2}$ correspond to the double-valued functions κ_v and κ_p, respectively. The poles $\omega = \pm\omega_s$ determine the excited partial surface wave. The integration path C_0 is the original inverse transform path along the real axis; C_1 and C_2 are the closed integration contours used for $\xi < 0$ and $\xi > 0$, respectively.

IV. TERAHERTZ SURFACE WAVES

With the solution in the Fourier domain at hand (7), (8), and (10a)–(10c), we now transform it to the usual ξ, x domain. In taking the inverse transforms of $\tilde{E}_y$,

$$E_y(x,y,\xi) = \int_{-\infty}^{\infty} dg \int_{C_0} d\omega\, e^{i\omega\xi - igx} \tilde{E}_y(\omega, g, y), \qquad (11)$$

we choose the integration path C_0 (see Fig. 3) along the entire real axis on the Riemann sheet in the complex ω plane, where the real parts of $\kappa_{v,p}(\omega)$ are positive to ensure decay of the fields at $y \to \pm\infty$. The branch cuts due to double-valued functions $\kappa_{v,p}(\omega)$ run along the real axis from the branch points $\pm\omega_1$, with $\omega_1 = c|g|(1-\beta^{-2})^{-1/2}$, and $\pm\omega_2$, with $\omega_2 = (c^2 g^2 + \varepsilon_0 \omega_p^2)^{1/2} (\varepsilon_0 - \beta^{-2})^{-1/2}$, to infinity. The path C_0 passes below the poles $\pm\omega_s$ of $\tilde{E}_y(\omega, g, y)$ and runs along the lower side of the branch cuts to satisfy the radiation condition $\omega \operatorname{Im} \kappa_{v,p} > 0$.

For the evaluation of the inverse transform on ω it is convenient to close the integration path C_0 in the lower half-plane for $\xi < 0$ (contour C_1 in Fig. 3) and in the upper half-plane for $\xi > 0$ (contour C_2 in Fig. 3). The contours $C_{1,2}$ are similar to that we used earlier in Ref. 17, but the poles and branch points are given by completely different expressions. When integrating along the contour C_1 (for $\xi < 0$), the entire response is given by the integrals along two semi-infinite straight lines tilted at an angle of 45° with the axes. These integrals contribute only to the near fields both in vacuum and in the semiconductor. When integrating along the contour C_2 (for $\xi > 0$), the integrals along the tilted lines contribute to the near fields, whereas integrals along the branch cuts on the real axis give the outgoing radiation in vacuum and in the semiconductor; the residue contributions at the poles $\pm\omega_s$ determine the excited partial (with definite g) surface wave. Additionally, in the semiconductor ($y < 0$) the electric field transform $\tilde{E}_y$ have poles at $\pm\omega_p$ [see Eq. (10b)] that describe Langmuir oscillations excited behind the optical spot. These oscillations are similar to the wakefield excited by a laser driver in the gaseous plasma in plasma-based accelerators.[18]

Let us focus on the excitation of the surface waves. The frequency of the partial surface wave is given by the position of the poles $\pm\omega_s$. Its amplitude is determined by the values of the residues calculated at the poles. The poles are given by the roots of the equation $\Delta(\omega) = 0$, i.e., $\varepsilon_p \kappa_v + \kappa_p = 0$, which is the well-known dispersion equation for surface waves. This equation can be reduced to the form

$$c^2 g^2 \omega^{-2} = \varepsilon_p (\varepsilon_p + 1)^{-1} - \beta^{-2}, \qquad (12)$$

and has two solutions $\omega = \pm\omega_s$. Using the relation between the components g and ω/V of the SPP's in-plane wave vector and the propagation angle φ, i.e., $g = \omega V^{-1} \cot\varphi$, it is convenient to express the frequency ω_s through the angle φ,

$$\omega_s = \bar{\omega}_p \sqrt{\frac{1 - \beta^2 \sin^2\varphi}{1 - \beta^2 \sin^2\varphi (1 + \varepsilon_0^{-1})^{-1}}}. \qquad (13)$$

Figure 2(b) shows the frequency ω_s as a function of the propagation angle φ for $\varepsilon_0 = 12.9$ (GaAs) and different β. The low-frequency SPPs, which are weakly localized and have large group velocities, propagate at large angles, $\varphi \to \alpha$. The waves with frequencies close to the largest possible frequency $\bar{\omega}_p$, which are strongly localized and have very small group velocities, propagate at $\varphi \approx 0$.

Summing the residue contributions from the poles $\omega = \pm\omega_s$ to the internal integral (11) and changing the integration variable $g \to \omega$ by use of Eq. (12) in the external integral (11), we arrive at the following expression for the electric field of the excited surface waves in vacuum ($y > 0$):

$$\begin{aligned} E_y^s(x,y,\xi) = {} & \frac{16\pi^2}{c^3} \int_0^{\bar{\omega}_p} d\omega \frac{\omega^3 \varepsilon_p^2 \tilde{G} |\tilde{F}| e^{-\kappa_v y}}{g(\varepsilon_p - 1)(\varepsilon_p + 1)^2} \\ & \times \sum_{\mp} \Bigg[\left(\frac{p_z}{\beta} \pm \frac{c g p_x}{\omega} \right) \cos(\omega\xi \mp gx - \psi) \\ & + \frac{p_y}{\sqrt{-\varepsilon_p - 1}} \sin(\omega\xi \mp gx - \psi) \Bigg], \end{aligned} \qquad (14)$$

where ψ is the phase of $\tilde{F}$ such that $\tilde{F}(\pm\omega) = |\tilde{F}| \exp(\mp i\psi)$ [$\psi = 0$ for the Gaussian pulse (2); see Eq. (6)]. The function $g(\omega)$ should be substituted into Eq. (14) from Eq. (12) (only positive g should be taken). The electric field of the surface waves in the semiconductor $E_y^s(x, y, \xi)$, $y < 0$, can be found from Eq. (14) by replacing $\exp(-\kappa_v y) \to \varepsilon_p^{-1} \exp(\kappa_p y)$.

Equation (14) gives the expansion of the electric field $E_y^s(x, y, \xi)$ into plane surface waves that propagate from the laser path to $x \to \pm\infty$ (outgoing waves) and toward the laser path (incoming waves). At large ξ, only the outgoing waves survive; the incoming waves interfere destructively. As a result, a farfield pattern of the outgoing radiation will be formed at large ξ. An asymptotic evaluation of the integral (14) for large ξ using the stationary phase method gives

$$E_y^s(x,y,\xi) \approx \frac{16\pi^2}{c^3}\sqrt{\frac{2\pi}{|g_0''x|}}\frac{\omega_0^3\varepsilon_{p0}^2\widetilde{G}_0|\widetilde{F}_0|e^{-\kappa_{v0}y}}{g_0(\varepsilon_{p0}-1)(\varepsilon_{p0}+1)^2} \times\Bigg[\left(\frac{p_z}{\beta}\pm\frac{cg_0p_x}{\omega_0}\right)\cos\Bigg[\omega_0\xi-g_0|x|-\psi_0 - \frac{\pi}{4}\mathrm{sgn}(g_0'')\Bigg]+\frac{p_y}{\sqrt{-\varepsilon_{p0}-1}}\sin\Bigg[\omega_0\xi-g_0|x|-\psi_0 - \frac{\pi}{4}\mathrm{sgn}(g_0'')\Bigg]\Bigg], \tag{15}$$

where the upper (lower) sign is taken for $x>0$ ($x<0$), g'' denotes the second derivative with respect to ω, and zero subscripts imply that all variables that depend on ω are taken at the frequency ω_0 for which

$$\frac{d}{d\omega}(\omega\xi - g|x| - \psi) = 0, \tag{16}$$

or (for $\psi=0$)

$$V\frac{dg}{d\omega} = \frac{V\xi}{|x|} = \cot\varphi. \tag{17}$$

In Eq. (17), φ is a half-apex angle of the cone with its apex on the moving laser pulse (Fig. 1); evidently, this angle coincides with the propagation angle of a partial plane wave. Figure 2(b) shows the stationary frequency ω_0 as a function of φ. For the cone that subtends the largest angle $\varphi=\alpha$, the frequency tends to zero, whereas $\omega_0 \to \bar{\omega}_p$ for $\varphi \to 0$. Thus, the frequency of surface waves arriving at a fixed observation point far from the laser path increases with time approaching asymptotically $\bar{\omega}_p$.

Typical distributions of the electric field $E_y(x,\xi)$ of the excited surface waves and near fields in the plane $y=0$ calculated on the basis of Eq. (11) for different orientations of $\mathbf{p}$, beam parameters $\ell_\perp$ and τ, and spot velocities β are shown in Fig. 4. The field distributions exhibit several interesting features. First, while for $\mathbf{p}$ oriented along $\hat{\mathbf{z}}$ the field pattern is symmetric with respect to $x=0$ (Fig. 4(a)), for $\mathbf{p}$ along $\hat{\mathbf{x}}+\hat{\mathbf{z}}$ it becomes strongly asymmetric (Fig. 4(b)). This allows one to control the direction of surface wave emission by varying the polarization of the optical beam or the beam's orientation relative to the crystallographic axes of the semiconductor. Interestingly, the symmetric radiation pattern is similar to that obtained in Ref. 8 for Cherenkov radiation in a homogeneous dispersive medium with a Lorentzian resonance. Second, the radiated fields behind the optical spot decrease in magnitude and fade more rapidly with ξ (for a fixed x) when the transverse size $\ell_\perp$ or/and duration τ of the laser pulse are increased (Figs. 4(c) and 4(d)). Finally, the opening angle of the Cherenkov cone increases if β approaches unity (Fig. 4(e)), in accord with the kinematic predictions of Sec. II.

To explain the dependence of the radiation pattern on the parameters of the laser pulse, it is necessary to study the spectral distribution of the radiated energy.

To find the total energy radiated into the surface waves per unit length of the laser path, we integrate the energy flux per unit area far from the laser path over infinite intervals of coordinate y ($-\infty < y < +\infty$) and time ξ ($0<\xi<\infty$). To find the $\pm x$-component of the Poynting vector $S_{\pm x} = \pm c(4\pi)^{-1}E_yB_z$, we use Eq. (14) and the inverse transform of $\widetilde{B}_z$. On integrating $S_{\pm x}$, we obtain the total energy radiated in $\pm x$ directions,

$$W_s^{\pm} = \int_0^{\bar{\omega}_p} w_s^{\pm}(\omega)d\omega, \tag{18}$$

where $w_s^{\pm}(\omega)$ is the spectral density of the radiation,

$$w_s^{\pm}(\omega) = \frac{32\pi^4\omega^4\varepsilon_p\widetilde{G}^2|\widetilde{F}|^2}{c^3g(\varepsilon_p^2-1)\sqrt{-\varepsilon_p-1}}\left[\frac{p_y^2}{\varepsilon_p+1} - \left(\frac{p_z}{\beta}\pm\frac{cgp_x}{\omega}\right)^2\right]. \tag{19}$$

According to Eq. (19), the energy radiated by the p_y component of the nonlinear polarization is added to the energy radiated by p_x and p_z ($\varepsilon_p < -1$ for surface waves). Thus, there is no interference between the surface waves radiated by p_y, on one hand, and $p_{x,z}$ on the other hand [see also Eq. (14)]. On the contrary, the waves emitted by the components p_x and p_z can interfere and produce an asymmetric radiation pattern (Fig. 4(b)) in which the energies radiated in $\pm x$ directions [Eq. (19)] differ significantly.

The spectral density of the radiated energy is shown in Fig. 5 for $\mathbf{p}=p\hat{\mathbf{z}}$ and different $\ell_\perp$ and τ. For $\mathbf{p}$ along $\hat{\mathbf{x}}$ and $\hat{\mathbf{y}}$, the spectrums are qualitatively similar. Figure 5(a) allows one to understand the distinctions between the radiation patterns shown in Figs. 4(a) and 4(c). Indeed, the total radiated energy (that is equal to the area under the curve of the spectral density in Fig. 5(a)) is less for $\omega_p\ell_\perp/c=10$ than for $\omega_p\ell_\perp/c=3$ (see also Fig. 6(a)). Furthermore, for $\omega_p\ell_\perp/c=10$ the plane waves with frequencies significantly smaller than $\bar{\omega}_p$ ($0.3 \leqslant \omega/\bar{\omega}_p \leqslant 0.7$) are predominantly excited. The group velocities of such waves (see dashed curve in Fig. 5(a)) are close to the speed of light and, therefore, the waves move rapidly from the laser path. For $\omega_p\ell_\perp/c=3$, the plane waves with frequencies close to $\bar{\omega}_p$ are excited efficiently. These waves have large transverse wave numbers $g(\omega)$ [see Eq. (12)] and small group velocities (Fig. 5(a)). The slowness of the emitted waves leads to the slowness of energy spreading in the lateral directions. This explains the slow fading of the oscillations near the laser path in Fig. 4(a). The slowness of the waves may affect an experimental observation of the radiation because collisional losses can attenuate the radiation before it reaches the receiver. When the laser width decreases below $\omega_p\ell_\perp/c \approx 3$, the peak in Fig. 5(a) narrows and moves closer to $\bar{\omega}_p$. Consequently, the total radiated energy drops rapidly (Fig. 6(a)) and the waves with negligible group velocities are excited.

Similarly, the dependence of the spectral density on τ shown in Fig. 5(b) explains the distinctions between the radiation patterns given in Figs. 4(a) and 4(d). For relatively long laser pulse with $\omega_p\tau=6$, the total radiated energy is less than for $\omega_p\tau=2$ (see also Fig. 6(a)) and the fast waves that leave rapidly the laser path are predominantly excited. In the

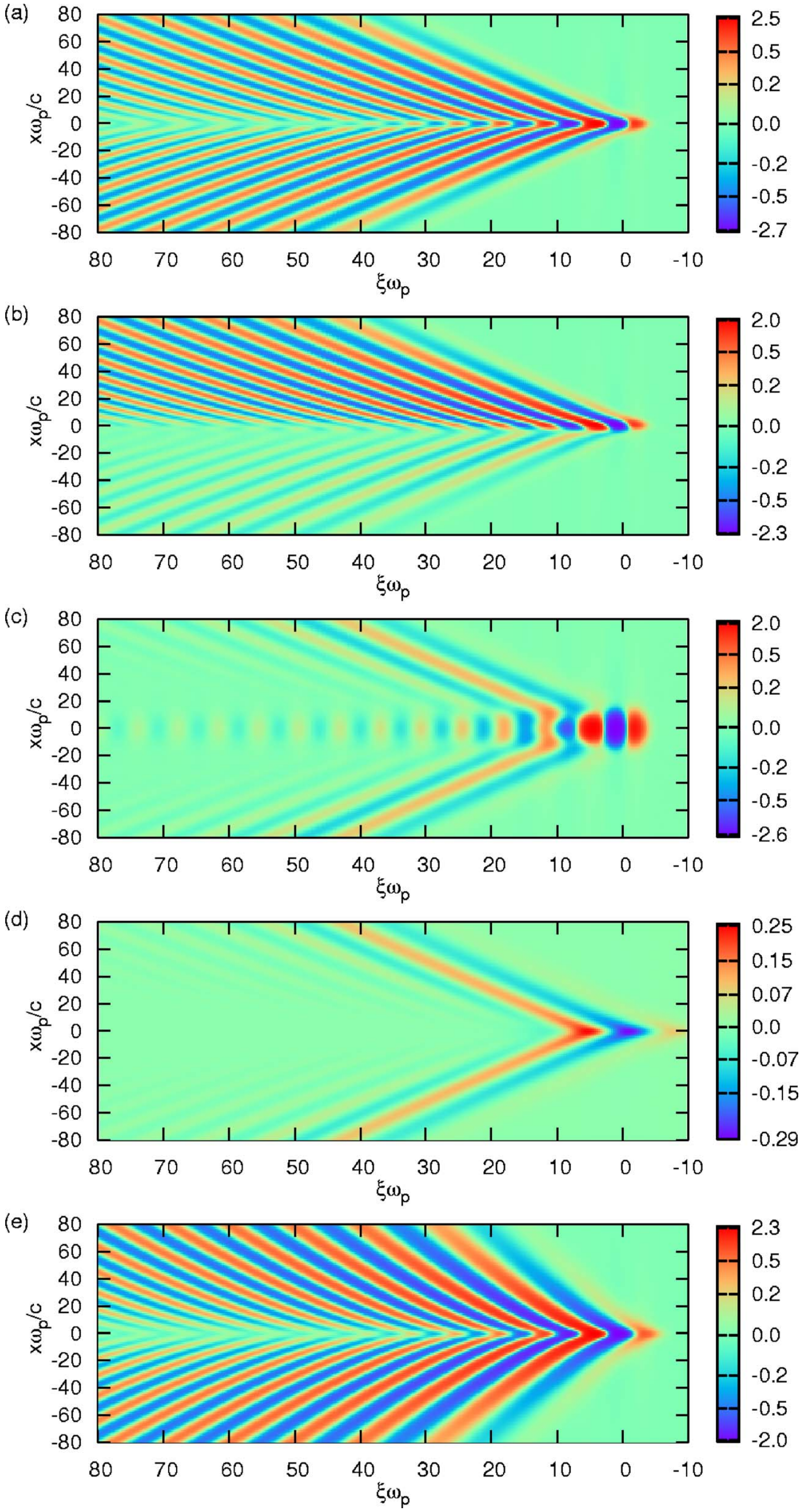

FIG. 4. (Color online) Snapshot of the electric field $E_y(x,\xi)$ at $y=0$ (normalized to $p\omega_p/c$) for (a) $\mathbf{p}=p\hat{\mathbf{z}}$, $\beta=1.1$, $\omega_p\ell_\perp/c=3$, $\omega_p\tau=2$; (b) the same as in (a) but $\mathbf{p}=p(\hat{\mathbf{x}}+\hat{\mathbf{z}})/\sqrt{2}$; (c) the same as in (a) but $\omega_p\ell_\perp/c=10$; (d) the same as in (a) but $\omega_p\tau=6$; (e) the same as in (a) but $\beta=1.02$. The background dielectric constant is $\varepsilon_0=12.9$ (GaAs).

opposite case, when the pulse duration decreases below $\omega_p\tau\approx 2$, the peak in Fig. 5(b) narrows, decreases in magnitude, and moves closer to $\bar{\omega}_p$. This results in a reduction of the total radiated energy (Fig. 6(a)) and a decrease of the group velocities of the excited waves (Fig. 5(a)).

Figure 6 shows that there exist optimal parameters $\ell_\perp$ and τ that can maximize the total radiated energy $W_s^{\pm}$. Interestingly, for $\mathbf{p}=p\hat{\mathbf{x}}$ and $\mathbf{p}=p\hat{\mathbf{y}}$ (not shown) the total radiated energy $W_s^{\pm}$ does not tend to zero when $\ell_\perp\to 0$ (Fig. 6(b)). This can be explained by an interplay of two processes: the infinite growth of the spectral density peak with $\ell_\perp\to 0$ and the shrinkage of the peak's width. However, this singularity

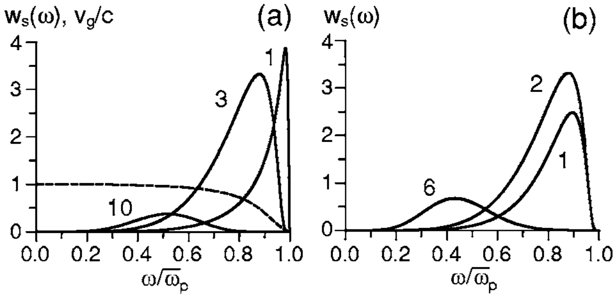

FIG. 5. Spectral density of the radiated energy $w_s^{\pm}(\omega)$ (normalized to $p^2/\bar\omega_p$) for (a) $\omega_p\tau=2$ and different values of $\omega_p\ell_\perp/c$ shown near corresponding curves; the dashed curve shows the group velocity v_g/c as a function of frequency; (b) $\omega_p\ell_\perp/c=3$ and different values of $\omega_p\tau$ shown near corresponding curves; the curve for $\omega_p\tau=6$ is magnified tenfold. The background dielectric constant is $\varepsilon_0=12.9$ (GaAs) and $\beta=1.1$.

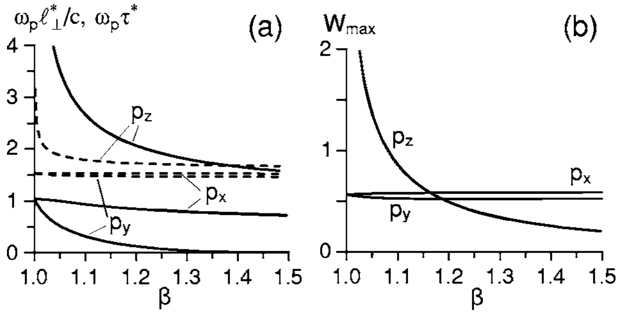

FIG. 7. (a) Optimal parameters $\omega_p\ell_\perp^*/c$ (solid lines) and $\omega_p\tau^*$ (dashed lines) maximizing the total radiated energy as functions of β for different components of $\mathbf{p}$ (shown near corresponding curves). (b) Maximal energy $W_{\max}$ (normalized to p^2) as a function of β when the spot polarization is p_x, p_y, or p_z.

of the spectral density has little application in practice because it occurs at $\omega\to\bar\omega_p$ and, therefore, corresponds to the excitation of the waves with negligible group velocity and high Ohmic losses (Sec. I). There is no such singularity for $\mathbf{p}=p\hat{\mathbf{z}}$; the magnitude of the peak in Fig. 5(a) tends to a finite value with $\ell_\perp\to 0$, and due to the narrowing of the peak, the total radiated energy tends to zero (Fig. 6(a)).

Figure 7 shows the optimal parameters $\ell_\perp^*$ and τ^* maximizing the radiated energy $W_s^{\pm}$ and the maximal energy $W_{\max}$ as functions of β for different orientations of the nonlinear polarization. One can conclude from Fig. 7 that the component p_z is the most appropriate for the excitation of THz surface waves. Indeed, for $\beta\leqslant 1.2$ the maximal energy is greater for p_z than for p_x or p_y. Furthermore, for p_x and p_y the optimal parameters are small: $\omega_p\ell_\perp^*/c<1$ and $\omega_p\tau^*<1.5$; therefore, the components p_x and p_y generate predominantly the waves with $\omega\approx\bar\omega_p$ and negligible group velocities (Fig. 5). These waves are of no practical interest due to their high damping.

We have discussed so far the properties of the generated SPPs for various orientations of the nonlinear polarization vector $\mathbf{p}$. Our next step is to relate $\mathbf{p}$ to the amplitude $\mathbf{E_0}$ of the electric field of the optical pulse and estimate the efficiency of the optical-to-terahertz conversion. We assume that the laser beam is p polarized. This polarization, according to the Fresnel formulas, provides a larger value of the electric field in the transmitted wave than s polarization. This is particularly important for grazing incidence ($\pi/2-\alpha\ll 1$), which is the regime we should use to get close-to-unity values of β (see above). Essentially, due to a rather high value of the refractive index n of GaAs at optical frequencies ($n\approx 3.7$ at 800 nm; the imaginary part is approximately ten times less) the refraction angle γ is small ($\gamma<16°$), even for grazing incidence. Therefore, the electric field $\mathbf{E_t}$ of the transmitted wave is almost parallel to the z axis ($E_{tz}\gg E_{ty}$, Fig. 8(a)). We relate $\mathbf{E_t}$ to $\mathbf{p}$ via the nonlinear optical susceptibility tensor (with the only nonzero components $d_{14}=d_{25}=d_{36}$)[19] and the penetration depth of the optical beam in the semiconductor ℓ_y. A (110) surface of GaAs seems to be the most appropriate for the observation of the physical effects predicted above for two reasons. First, by changing the azimuthal angle θ (Fig. 8(a)) this surface allows one to maximize $|p_z|$ at $\theta\approx 55°$ (Fig. 8(b)) to get the maximal energy yield. Second, it can provide $p_x=p_z$, $p_y\approx 0$ at $\theta\approx 75°$ (Fig. 8(b)) to create an asymmetric radiation pattern (Fig. 4(b)) and more directional emission.

To estimate the conversion efficiency it is convenient to introduce the coefficient η_s that relates the energy W_s of SPPs and the peak intensity I_0 of the incident laser pulse,

$$W_s = W_s^+ + W_s^- = \eta_s I_0^2, \quad \text{with } I_0 = \frac{c}{8\pi}E_0^2. \tag{20}$$

Figure 9(a) shows the coefficient η_s as a function of the incident angle α for the case of the optimal orientation of GaAs crystal $\theta=55°$ and for $\omega_p/2\pi=8$ THz (doping concentration $N\approx 6.4\times 10^{17}\ \mathrm{cm}^{-3}$), $\omega_p\ell_\perp/c=10$ ($\ell_{\perp\mathrm{FWHM}}=2\sqrt{\ln 2}\,\ell_\perp\approx 100\ \mu\mathrm{m}$), and $\omega_p\tau=2$ ($\tau_{\mathrm{FWHM}}\approx 66$ fs). The

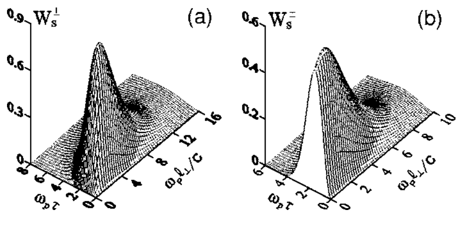

FIG. 6. The total radiated energy $W_s^{\pm}$ (normalized to p^2) as a function of $\ell_\perp$ and τ for: (a) $\mathbf{p}=p\hat{\mathbf{z}}$; (b) $\mathbf{p}=p\hat{\mathbf{x}}$. The background dielectric constant is $\varepsilon_0=12.9$ (GaAs) and $\beta=1.1$.

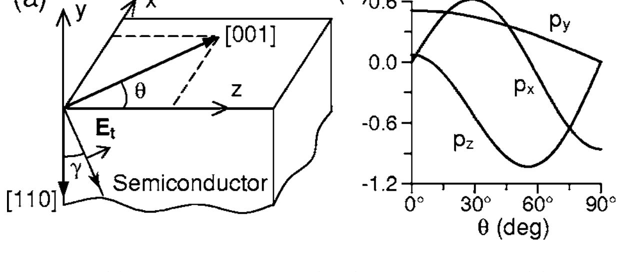

FIG. 8. (a) Geometry of the (110) GaAs surface. (b) Components of the vector $\mathbf{p}$ (normalized to $d_{14}E_t^2\ell_y$) as functions of the azimuthal angle θ.

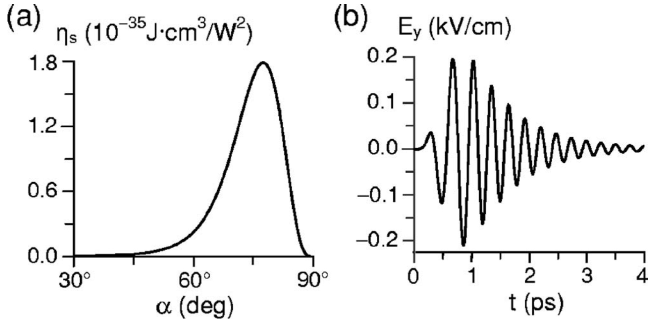

FIG. 9. (a) The coefficient η_s as a function of the incident angle α. (b) Oscillogram $E_y(t)$ at $x=50c/\omega_p$, $y=0$, and $z=0$ for $\alpha=78^\circ$ ($\beta=1.02$). The other parameters for both figures are specified in the text.

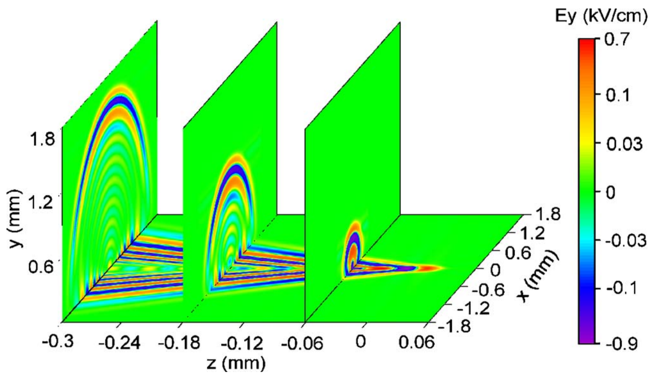

FIG. 10. (Color online) Snapshot ($t=0$) of the electric field $E_y(x,y,z)$ on the GaAs surface ($y=0$) and in the vacuum ($y>0$) for the same parameters as in Fig. 9(b).

transmission of the incident field to the semiconductor ($n=3.7$ for GaAs) was calculated using the Fresnel formulas. We also used $d_{14}=66$ pm/V[20,21] and $\ell_y=1$ μm.[22] The function $\eta_s(\alpha)$ reaches a maximum $\eta_s \approx 1.8\times10^{-35}$ J cm^3/W^2 at $\alpha\approx78^\circ$ ($\beta\approx1.02$). Thus, for a laser intensity of $I_0=50$ GW/cm^2, we can obtain a rather high energy $W_s\approx4.6\times10^{-14}$ J/cm and conversion efficiency $W_s/W_i\approx6\times10^{-9}$ of the incident optical energy $W_i=I_0\pi\ell_\perp\tau\cos\alpha$. This efficiency is less than the one reported in the literature for the free-space radiation.[21] However, the energy density of the surface waves decays with the distance from the surface. Therefore, the electric field on the surface can be rather strong. Figure 9(b) shows the oscillogram of the field $E_y(t)$ at $x=50c/\omega_p$, $y=0$, and $z=0$ for $\beta=1.02$; the other parameters are the same as for Fig. 9(a). In Fig. 9(b), the field strength reaches a rather high magnitude of 0.2 kV/cm. Figure 9(b) also shows that the frequency of the oscillations increases noticeably with time in the beginning of the oscillogram and then remains constant. This is in accord with the prediction of the stationary phase method (Fig. 2(b)).

V. TERAHERTZ FREE-SPACE RADIATION

In the previous section we discussed the kinematic properties and excitation efficiencies for the surface waves that spread from the path of the optical spot but remain confined to the surface. In addition to these waves, the spot will generate waves that will leave the surface and produce free-space radiation both in the semiconductor and in vacuum. These waves will form a Cherenkov cone that is asymmetric with respect to the $y=0$ plane. All properties of the free-space radiation are described by the integral along the branch cuts along the real axis of the integration contour shown in Fig. 3. Figure 10 shows a typical distribution of E_y on the surface and in vacuum. At small distances from the spot, the surface and free-space waves interfere significantly and cannot be separated. At large distances they become separated and form two radiation patterns.

By integrating the Poynting vector of the free-space radiation emitted in the ±x directions in vacuum and representing the radiated energy as $W_v=\eta_v I_0^2$, we can compare the conversion efficiency for these waves with that for the surface waves. The efficiencies as functions of the incident angle α are plotted in Fig. 11. Almost for the whole range of α the energy emitted into vacuum exceeds that of the surface waves. This difference is particularly large for small angles when the optical spot moves with the velocity exceeding significantly the speed of light ($V/c\to\infty$ when $\alpha\to0$). This limit corresponds to the case when the spot creates instantaneously a line of nonlinear polarization. The line emits radiation that propagates almost perpendicularly to it, i.e., the cone angle approaches zero. The low excitation efficiency for the surface waves in the limit $\alpha\to0$ can easily be explained. The instantaneously created line produces surface waves that propagate in the ±x directions. The electric field of such waves has only x and y components. Therefore, these waves cannot be excited by the z-polarized source. However, at grazing incidence the energy of the surface waves becomes comparable to that emitted in vacuum and can even exceed it slightly.

VI. CONCLUSION

To conclude, we have predicted and analyzed the excitation of THz surface waves on a semiconductor surface by a short optical pulse. The pulse was assumed to be focused in one direction and produce an optical spot that moves along the surface with superluminal velocity. The presence of nonlinearities in the semiconductor should give rise to a moving

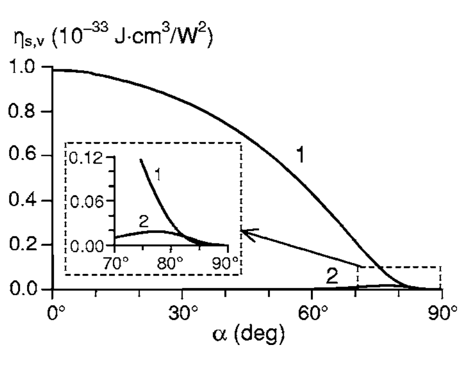

FIG. 11. The coefficient η_v (curve 1) as a function of the incident angle α for the same parameters as in Fig. 9(a). The dependence $\eta_s(\alpha)$ (curve 2) is shown for comparison.

pulse of nonlinear polarization, which in turn will emit Cherenkov waves in the THz spectral range. By doping the semiconductor one can introduce SPPs that will be excited as part of the Cherenkov radiation.

In the present paper, we assumed that nonlinearity comes from optical rectification in bulk. This allowed us to estimate the excitation efficiency and to find the orientation of the surface and incident angles that give the most efficient excitation of the surface waves. However, the possibility to excite THz surface waves is not limited to optical rectification and will exist in many other situations when the spot creates a time-dependent variation in polarization on the picosecond scale. Among those, we mention surface-induced optical rectification[5,23] or ultrafast current creation.[1–3] In the latter case, the source would be a spatiotemporal distribution of surface currents rather than a moving pulse of nonlinear polarization. While the theory developed in this paper describes the excitation of surface waves for all the mentioned mechanisms, the excitation efficiencies will differ. We also emphasize that the generated surface wave does not have to be a SPP, the case treated in the paper. The excitation scheme and developed theory are applicable to other surface waves, for example, surface phonon polaritons and surface exciton polaritons.

Finally, the proposed technique, in addition to its potential use as a THz source, can be a useful tool to study THz properties of clean semiconductor surfaces as well as to probe the properties of materials deposited on surfaces.

This work was supported in part (M.I.B. and S.B.B.) by the program ”Femtosecond optics and physics of superstrong laser fields” of the Presidium of RAS. The work of A.V.M. was supported by a NASA grant to ELORET Corporation (Sunnyvale, California).

---

[1] P. R. Smith, D. H. Auston, and M. C. Nuss, IEEE J. Quantum Electron. **24**, 255 (1988).

[2] X.-C. Zhang, B. B. Hu, J. T. Darrow, and D. H. Auston, Appl. Phys. Lett. **56**, 1011 (1990).

[3] T. Dekorsy, H. Auer, H. J. Bakker, H. G. Roskos, and H. Kurz, Phys. Rev. B **53**, 4005 (1996).

[4] S. L. Chuang, S. Schmitt-Rink, B. I. Greene, P. N. Saeta, and A. F. J. Levi, Phys. Rev. Lett. **68**, 102 (1992); P. N. Saeta, B. I. Greene, and S. L. Chuang, Appl. Phys. Lett. **63**, 3482 (1993).

[5] R. Adomavičius, A. Urbanowicz, G. Molis, A. Krotkus, and E. Šatkovskis, Appl. Phys. Lett. **85**, 2463 (2004).

[6] D. H. Auston, K. P. Cheung, J. A. Valdmanis, and D. A. Kleinman, Phys. Rev. Lett. **53**, 1555 (1984).

[7] G. A. Askar’yan, Zh. Eksp. Teor. Fiz. **42**, 1360 (1962) [Sov. Phys. JETP **15**, 943 (1962)]; Phys. Rev. Lett. **57**, 2470 (1986).

[8] T. E. Stevens, J. K. Wahlstrand, J. Kuhl, and R. Merlin, Science **291**, 627 (2001).

[9] J. K. Wahlstrand and R. Merlin, Phys. Rev. B **68**, 054301 (2003).

[10] M. Schall, H. Helm, and S. R. Koiding, Int. J. Infrared Millim. Waves **20**, 595 (1999).

[11] A. G. Stepanov, J. Hebling, and J. Kuhl, Opt. Express **12**, 4650 (2004).

[12] *Electromagnetic Surface Modes*, edited by A. D. Boardman (Wiley, New York, 1982); V. M. Agranovich and V. L. Ginzburg, *Crystal Optics with Spatial Dispersion and Excitons* (Springer-Verlag, Berlin, 1984), Chap. 5.

[13] B. Liedberg, C. Nylander, and I. Lundstrom, Biosens. Bioelectron. **10** (8), i (1995).

[14] R. J. Bussjager and H. A. Macleod, Appl. Opt. **35**, 5044 (1996).

[15] S. I. Bozhevolnyi and F. A. Pudonin, Phys. Rev. Lett. **78**, 2823 (1997); H. Ditlbacher, J. R. Krenn, G. Schilder, A. Leitner, and F. R. Aussenegg, Appl. Phys. Lett. **81**, 1762 (2002).

[16] M. I. Bakunov, A. V. Maslov, S. B. Bodrov, and M. Hangyo, *Conf. Digest of the 2004 Joint 29th Int. Conf. Infrared and Millimeter Waves and 12th Int. Conf. Terahertz Electron.*, Karlsruhe, Germany, 27 September–1 October 2004, p. 357.

[17] M. I. Bakunov, A. V. Maslov, and S. B. Bodrov, J. Appl. Phys. **98**, 033101 (2005).

[18] E. Esarey, P. Sprangle, J. Krall, and A. Ting, IEEE Trans. Plasma Sci. **24**, 252 (1996).

[19] Q. Chen, M. Tani, Z. Jiang, and X.-C. Zhang, J. Opt. Soc. Am. B **18**, 823 (2001).

[20] W. D. Johnston, Jr., and I. P. Kaminow, Phys. Rev. **188**, 1209 (1969).

[21] J. Hebling, A. G. Stepanov, G. Almasi, B. Bartal, and J. Kuhl, Appl. Phys. B **78**, 593 (2004).

[22] M. Schall and P. U. Jepsen, Opt. Lett. **25**, 13 (2000).

[23] M. Reid, I. V. Cravetchi, and R. Fedosejevs, Phys. Rev. B **72**, 035201 (2005).